coatings

MDPI

Article

# The Influence of Aluminizing Process on the Surface Condition and Oxidation Resistance of Ti–45Al–8Nb–0.5(B, C) Alloy

**Wojciech Szkliniarz [1], Grzegorz Moskal [1], Agnieszka Szkliniarz [1,*] and Radosław Swadźba [2]**

[1] Faculty of Materials Engineering and Metallurgy, Institute of Materials Engineering, 40-019 Katowice, Poland; wojciech.szkliniarz@polsl.pl (W.S.); grzegorz.moskal@polsl.pl (G.M.)
[2] Institute for Ferrous Metallurgy, 44-100 Gliwice, Poland; rswadzba@imz.pl
* Correspondence: agnieszka.szkliniarz@polsl.pl; Tel.: +48-32-603-4400

Received: 3 March 2018; Accepted: 19 March 2018; Published: 20 March 2018

**Abstract:** One of the major barriers limiting the suitability of TiAl intermetallic alloys for use in the demanding aircraft and automotive industries is their susceptibility to degradation as a result of oxidation at temperatures exceeding 760 °C. Paper presents the characteristics of resistance to cyclic oxidation at 950 °C for Ti–45Al–8Nb–0.5(B, C) alloy with and without protective coating obtained as a result of aluminizing using out of pack method. The characteristics of surface condition were determined by scanning electron microscope with EDS system, transmission electron microscope, and X-ray diffractometer. The favorable behavior of the Ti–45Al–8Nb–0.5(B, C) alloy with a protective coating under cyclic oxidation conditions is a result of a higher content of $Al_2O_3$ in the microstructure of the scale and the presence of Al and Nb-rich phases at the substrate interface, which probably constitue a barrier for oxidation process. The high temperature oxidation test revealed that aluminide coating was responsible for a remarkable improvement in the oxidation resistance.

**Keywords:** TiAl–based alloys; aluminide coating; aluminization process; cyclic oxidation resistance; surface characterization

## 1. Introduction

Ordered intermetallic TiAl-based alloys are characterized by low density, high stiffness and relatively good strength, good creep and oxidation resistance, as well as low susceptibility to self-ignition. They belong to the new generation construction materials suitable for operating under temperatures in the range from 600 to 750 °C [1–5]. They can be successfully applied to the rotating components of modern aircraft engines (e.g., low pressure turbine blades and high pressure compressor blades), the moveable construction components of combustion engines (e.g., valves and turbocharger impellers), and as blades of gas turbines more commonly applied in power generation industry [1–7]. However, low ductility of intermetallic TiAl-based alloys at temperatures lower than 600 °C and lack of sufficient high temperature oxidation resistance above 750 °C are the main obstacles for a broader application of these materials [3–5,8].

Under high-temperature oxidation conditions, TiAl-based alloys do not form a protective $Al_2O_3$ scale that would be a barrier from further oxidation, but instead a mixture of $TiO_2$ and $Al_2O_3$ is formed. Such a scale does not represent sufficient protective properties due to much higher kinetics of $TiO_2$ growth and its lower adhesion to the surface [5,9,10]. The $TiO_2$ grows rapidly due to considerably easier oxygen diffusion through its defected anion sublattice by vacancy mechanism in contrast to $Al_2O_3$ [8–11].

The oxidation rate of TiAl-based alloys can be lowered by additions such as niobium, tungsten, molybdenum, tantalum, chromium, hafnium, and silicon [4,5,9,11–13]. The most effective of the

aforementioned elements is niobium, which, in addition to improving oxidation resistance, increases also the creep resistance and mechanical properties at room and elevated temperatures. Introduction of niobium (up to 10 at.%) to TiAl-based alloys leads to a decrease in their oxidation rate. The detailed mechanism of this niobium effect has not been fully explained. In Nb-doped alloys, the scale formed during high temperature oxidation contains $(Ti,Nb)O_2$ instead of $TiO_2$, in which part of the tetravalent $Ti^{4+}$ cations are replaced by pentavalent $Nb^{5+}$. Compared to $TiO_2$, it is characterized by a lower oxygen vacancy density, and thus it is more compact and chemically uniform and, as a consequence, its protective properties are higher. The presence of niobium influences also the higher aluminum activity and lowers oxygen solubility in the alloy, as well as promoting the formation of a continuous protective layer of nitrides at the scale–metal interface and interlayers rich in niobium and other alloying components.

II generation TiAl-based alloys include i.a. Ti–48Al–2Cr–2Nb, which recently has been successfully applied for low pressure turbine blades in aircraft engines [5,6] and Ti–47Al–2W–0.5Si [14] cast alloy, whose operating temperature does not exceed 760 °C. The development of III generation TNB alloys resulted in temperature capabilities enhancement to 800–850 °C [3,5,13] owing to addition of niobium (up to 10 at.%). Increasing the acceptable operating temperature of TiAl-based alloys to 950 °C would significantly broaden their application as an alternative to expensive and heavy nickel superalloys; however, this improvement requires the usage of protective coatings [9,15–22].

The oxidation protection of TiAl-based alloys may be obtained by the application of coatings such as MCrAlY [17]; aluminide coatings based on Al-rich $TiAl_2$ and $TiAl_3$ phases [18]; silicon modified aluminide coatings; and $Al_2O_3$-, $SiO_2$-, and $CaTiO_3$-based coatings [19–22]. One of the most interesting ways to increase the high temperature resistance of the TiAl-based alloys is through the deposition of the $Ni_2Al_3$ layer, which, under high temperature oxidation conditions, forms a protective $Al_2O_3$ scale [23]. The deposition of coatings is performed using such methods as ion implantation, sputtering and magnetron sputtering, plasma spraying, slurry, sol-gel, Chemical Vapor Deposition and Physical Vapor Deposition (Arc-PVD and EB-PVD), and diffusion aluminizing using one of the oldest and most commonly applied pack cementation method, as well as the out of pack method [4,9,15–25].

The advantage of the out-of-pack aluminizing method is the fact that components are placed in a container, and thus they have no contact with the powder mixture. The specimens are heated in a retort or vacuum furnace. During the process of coating deposition, the container is filled by inert carrier gas, which allows the transference of coat-forming gases created during the process to coated material. The substantial profit of the out-of-pack method is lack of contact between the substrate material and powder, resulting in notable improvement of coating surface. The control of process, as well as purity, is considerably increased, compared to powder technologies. Furthermore, this method allows improvement of oxidation resistance due to the possibility of modification of aluminide coatings, as well as the fact that aluminide diffusion coatings may be modified by various elements [4,26].

The aim of the investigation was to characterize the cyclic oxidation resistance of the uncoated Ti–45Al–8Nb–0.5(B, C) alloy with the aluminide protective coating obtained by "out of pack" method.

## 2. Materials and Methods

The chemical composition of the investigated Ti–45Al–8Nb–0.5(B, C) alloy is presented in Table 1. This alloy represented a III generation of TiAl-based alloy and, compared to the most popular II generation alloys such as Ti–48Al–2Cr–2Nb and Ti–47Al–2W–0.5Si, it is characterized by an elevated strength and significantly higher creep and oxidation resistance with sufficient ductility and toughness.

**Table 1.** Chemical composition of researched alloy.

| Element | Chemical Composition |
|---|---|
| Al | 44.25 at.% |
| Nb | 7.34 at.% |
| B | 0.15 at.% |
| C | 0.34 at.% |
| O | 935 ppm |
| N | 96 ppm |
| H | 17 ppm |
| Ti | Balance |

The investigated alloy was prepared from the commercial pure Ti (Grade 1), as well as Al, Nb, C, and B, which were added accordingly as Al-Nb master alloy, anthracite, and crystalline boron. The melting of TiAl-based alloy was performed in vacuum induction furnace using a special isostatic pressed graphite crucible [25,27,28]. Subsequently, alloy was cast into a graphite mold. The final cast had a form of an ingot with dimensions ϕ 45 mm and approx. 350 mm length. After 4 h of vacuum homogenizing treatment at temperature 1400 °C, the ingot was subjected to hot isostatic pressing (HIP) at 1260 °C and 170 MPa for 1 h under protection of highest purity argon.

Cylindrical test samples of ϕ 14 mm and 4 mm height were cut from ingot. The surface was covered by protective coating, obtained by out-of-pack aluminizng method, which was performed at Surface Engineering Laboratory in Institute of Materials Science at Silesian University of Technology. The aluminide coatings were brought at 900 °C for 5 h under Ar atmosphere. To evaluate the oxidation resistance of the bare and coated alloy, the cyclic oxidation test was conducted at the temperature of 950 °C, which is in accordance with the desired most rigorous operating conditions concerning this group of alloys. The first step in procedure was placement of test samples into the furnace with desired test temperature. Cyclic oxidation test was conducted for 100 cycles. Each cycle lasted 23 h at 950 °C, followed by 1 h air cooling to room temperature. The oxidation behavior in form of the curves of weight gain was determined via measuring the mass gain per area with 0.0001 g resolution, with every following cycle. The microstructure characterization was performed using microscopic observations (Nikon SMZ 745T, Tokyo, Japan) and scanning electron microscopy (Hitachi 3400N (Tokyo, Japan) with the Noran System 7 software v. 3.0). The samples designated for microstructure evaluation were mechanically polished and etched in solution composed of 30 mL of lactic acid, 15 mL of $HNO_3$, and 5 mL of HF. The microstructural evaluation of alloy substrate, obtained coating and oxide scale, was performed on the cross section of samples. The JEOL JDX 7S diffractometer (JEOL, Tokyo, Japan) was used for the X-ray diffraction (XRD) analysis of coating layer in order to yield the phase composition of the obtained coating. The chemical composition of aluminized surface was determined via energy dispersive X-ray (EDX) spectrometry microanalysis. TEM investigation was performed on FEI TITAN 80–300 transmission electron microscope (FEI, Hillsboro, OR, USA). Specimens for TEM were prepared by means of ion beam thinning and twin jet polishing using a reagent containing 30 mL of $HClO_4$, 175 mL of butony-ethanol, and 300 mL of $CH_3OH$. Over the course of polishing, the maintained voltage value was 15 V.

## 3. Results and Discussion

Figure 1 presents the microstructure of researched Ti–45Al–8Nb–0.5(B, C) alloy after homogenizing and hot isostatic pressing. The microstructure of the investigated alloy in an initial state contains grains of the primary α phase, characterized by moderate size. Grains were composed of plate-shaped precipitates of $\alpha_2$-$Ti_3Al$ phase with hexagonal $DO_{19}$ structure and γ-TiAl phases with tetragonal $L1_0$ structure, which were alternately arranged and characterized by interlamellar spacing of approx. 0.5 μm. Phase composition analysis performed by XRD revealed the prevalent content of the γ-TiAl phase in the duplex microstructure of the alloy (Figure 2). Transmission electron microscopy and

electron diffraction investigations of the Ti–45Al–8Nb–0.5(B, C) disclosed the presence of fine $Ti_3AlC_2$ carbide precipitates of regular size (Figure 3) that are responsible for both solution and precipitate strengthening effect, and also $Ti_2B_5$ boride precipitates of irregular shape (Figure 4), as well as elongated $Nb_3B_2$ (Figure 5) that cause grain refinement.

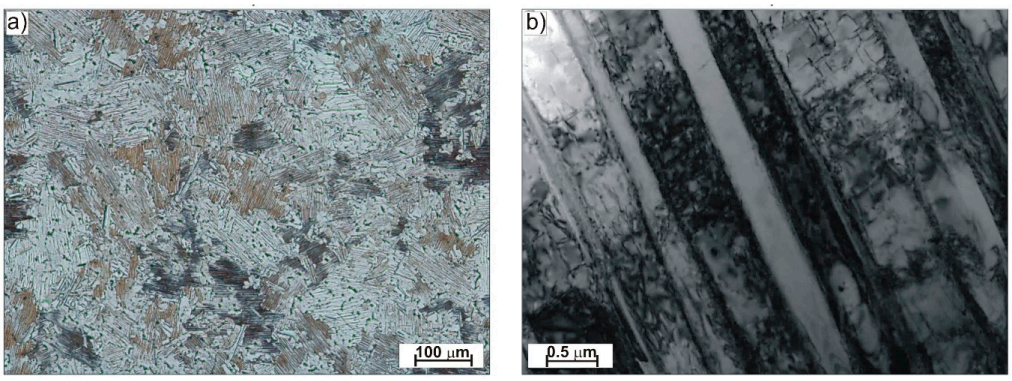


**Figure 1.** Microstructure of the Ti–45Al–8Nb–0.5(B, C) alloy—initial state: (**a**) LM, (**b**) TEM.

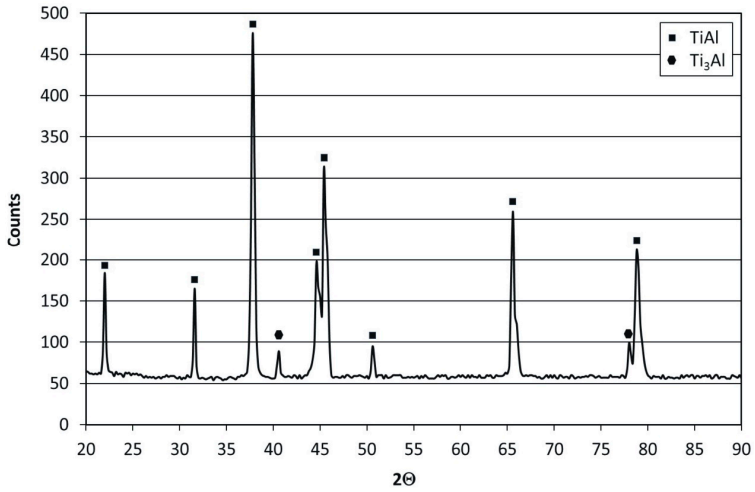


**Figure 2.** X-ray diffractogram of the Ti–45Al–8Nb–0.5(B, C) alloy—initial state.

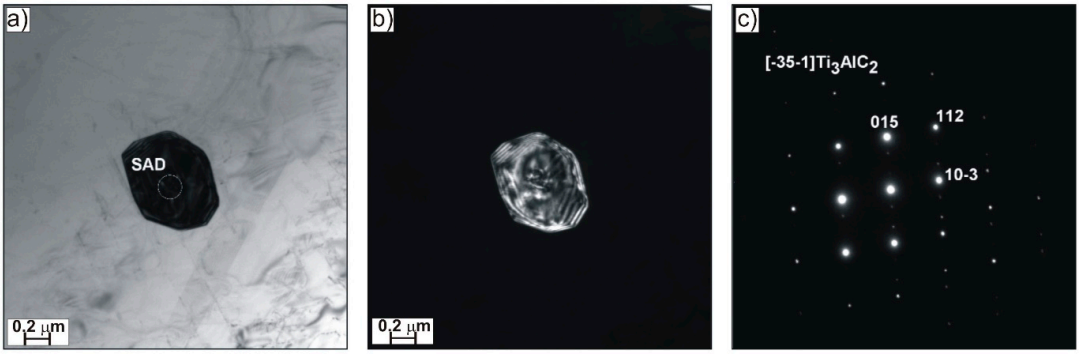


**Figure 3.** $Ti_3AlC_2$ phase precipitates in the Ti–45Al–8Nb–0.5(B, C) alloy: bright field (**a**), dark field (**b**), and electron diffraction (**c**).

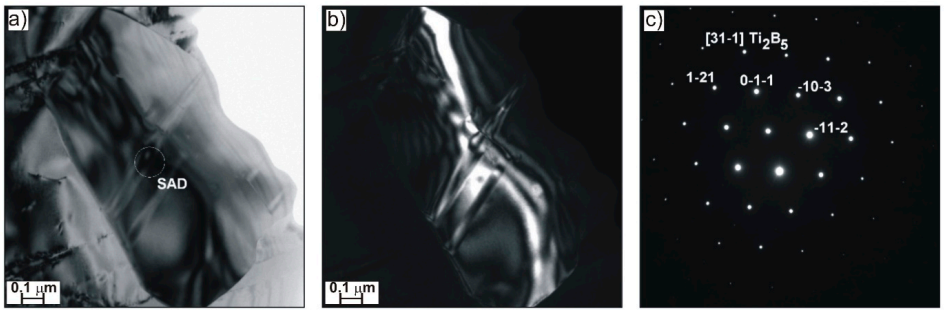


**Figure 4.** $Ti_2B_5$ phase precipitates in Ti–45Al–8Nb–0.5(B, C) alloy: bright field (**a**), dark field (**b**), and electron diffraction (**c**).

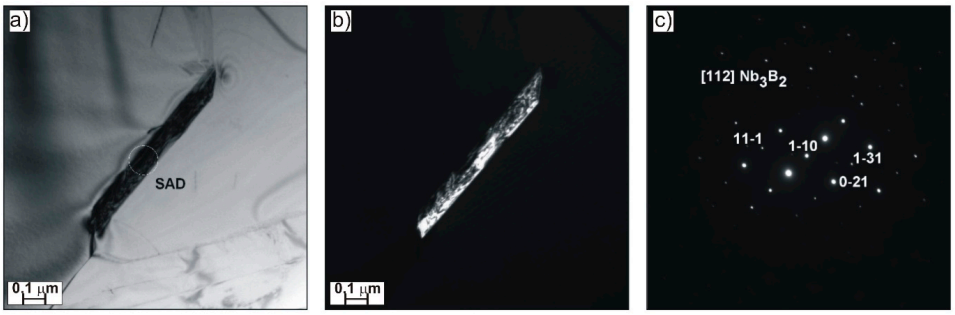


**Figure 5.** $Nb_3B_2$ phase precipitates in the Ti-45Al-8Nb-0.5(B, C) alloy: bright field (**a**), dark field (**b**), and electron diffraction (**c**).

During the diffusion aluminizing process, a compact protective coating was obtained on the Ti–45Al–8Nb–0.5(B, C) alloy. It is characterized by a uniform thickness of layer, which was approx. 8 μm (Figure 6). It was revealed that the coating consists of a single zone with fine grained structure and numerous fine precipitates on the grain boundaries of the matrix, which are not present in the substrate alloy (Figure 6). The distribution of the precipitates within the coating suggests that they inherit the orientation of the initial plate-like structure of the substrate alloy, which indicates inward diffusion of aluminum. The outer bright layer visible in Figure 6 is the Ni–P coating deposited in order to protect the aluminide coating during metallographic sample preparation. The line profiles illustrating the distribution of elements in the cross-section of the coating (Figure 7) indicate that in comparison to the substrate alloy, it is enriched in Al and depleted in Ti and Nb.

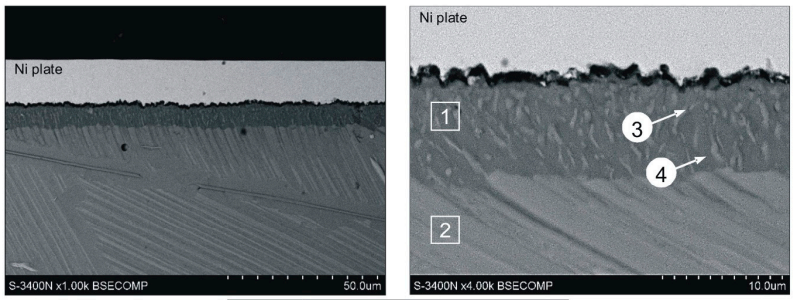


| Area Point | Elements content, at.% | | |
|---|---|---|---|
| | Ti | Al | Nb |
| 1 | 30.7 | 63.8 | 5.5 |
| 2 | 45.5 | 46.3 | 8.2 |
| 3 | 27.6 | 65.2 | 7.2 |
| 4 | 31.5 | 62.8 | 5.7 |

**Figure 6.** The microstructure (SEM) and chemical composition of the marked areas (points 1–4) in the diffusion aluminide coating on Ti–45Al–8Nb–0.5(B, C) alloy obtained using vapor aluminizing.

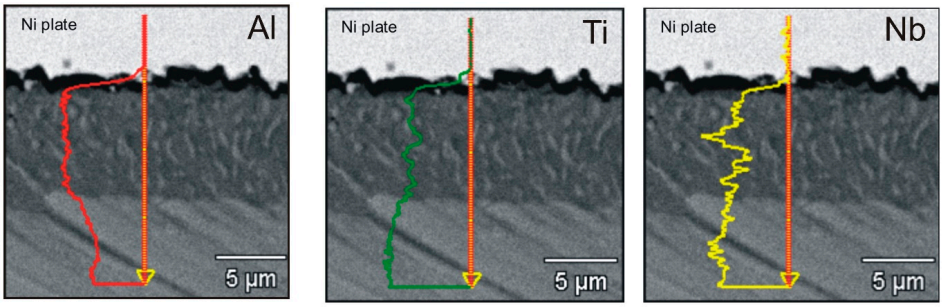


**Figure 7.** Linear distribution of Al, Ti, and Nb of cross-section of Ti–45Al–8Nb–0.5(B, C) alloy modified aluminium coating.

Quantitative analysis of chemical composition of the substrate alloy (point 2 in Figure 6) revealed that the Al/Ti content ratio is close to 1. However, the average content of aluminum in the aluminide coating (point 1 in Figure 6) is 17.5 at.% higher compared to the substrate, which indicates the aluminum to titanium content ratio is 2:1. As result, the substrate predominant phase is TiAl, while in the coating it is Al-rich $Al_2Ti$ phase. The niobium content in the coating is lower than in the substrate.

Detailed analysis of chemical composition of the precipitates present in the grain boundaries of the coating indicates that, compared to the matrix, they are characterized by a higher niobium and aluminum content and lower titanium content (points 3 and 4 in Figure 6).

X-ray diffraction phase composition analysis of the coating deposited on Ti–45Al–8Nb–0.5(B, C) alloy confirmed previous findings obtained using chemical composition microanalysis (Figure 8) and revealed the presence of three intermetallic phases from the Ti–Al system: predominant $Al_2Ti$ phase, relatively Al-poorer TiAl phase, and Al-rich $Al_3Ti$ phase. The correlation of the XRD and EDS results indicates the presence of $Ti(Al,Nb)_3$ instead of $Al_3Ti$ phase in which the ratio of Ti content to Al + Nb content is 1:3 visible in the form of fine Nb-rich precipitates in Figure 6.

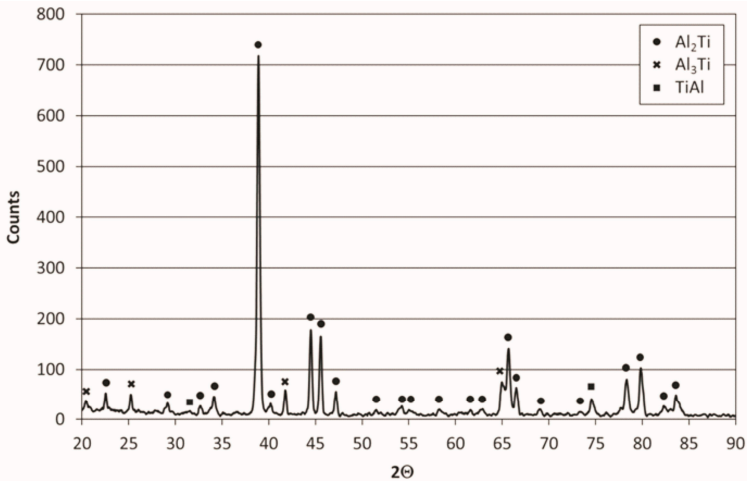


**Figure 8.** X-ray diffractograms of Ti–45Al–8Nb–0.5(B, C) alloy modified aluminium coating.

The results of cyclic oxidation resistance test at 950 °C of the bare and coated Ti–45Al–8Nb–0.5(B, C) alloy obtained in 23 h cycles with 1 h cooling to room temperature are presented in Figure 9. Under cyclic oxidation conditions, the bare alloy undergoes an intensive mass increase within the first 9 cycles, which is caused by the growth of olive-colored scale on its surface. The mass change curve between 10 and 21 cycles is characterized by a typical effect of scale spallation and healing. More pronounced scale spallation leading to exposure of the substrate material increases the rate of degradation, and after 22 cycles a rapid mass loss of the alloy is observed. After 23 cycles, the mass of the alloy dropped below its

initial value. In summary, the as-cast Ti–45Al–8Nb–0.5(B, C) alloy after homogenizing and hot isostatic pressing, exposed to oxidation under cyclic conditions at 950 °C, was characterized by a high mass growth followed by a rapid drop, high propensity for scale spallation, and a limited ability to heal. Compared to cast Ti–47Al–2W–0.5Si alloy, which was the subject of previous researches, the investigated alloy reveals slightly better oxidation resistance [25]. Although the addition of both tungsten and silicon improve the high-temperature oxidation resistance, under the same cyclic oxidation conditions, Ti–47Al–2W–0.5Si alloy revealed very high weight gain only until completion of seventh cycle. The reduction of alloy weight resulting from poor scale adhesion to the substrate, as well as fall-off effect, was observed starting from the tenth cycle. The number of cycles in case of investigated alloy was almost 2 times larger.

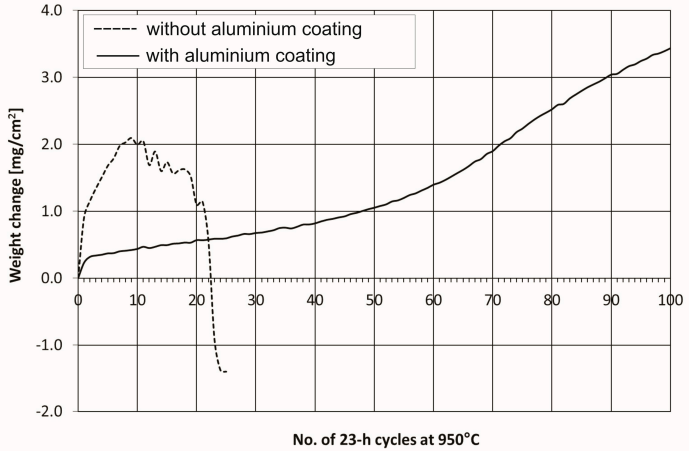


**Figure 9.** Mass change vs number of cycles at 950 °C for the bare and aluminium coated Ti–45Al–8Nb–0.5(B, C) alloy.

The scale formed on the surface of the Ti–45Al–8Nb–0.5(B, C) alloy after 25 cycles at 950 °C is double layered, and each of the layers is characterized by a morphology typical for a mixture of different oxides (Figure 10). The thickness of the scale is between 20 and 30 µm. Chemical composition analysis of the bright areas 1, 2, and 4 marked in Figure 10 revealed an elevated content of titanium, while in the dark gray region marked as 3 the aluminum is predominant. Underneath the oxide scale there is a layer containing Nb-rich precipitates (point 5 in Figure 10) and Al-rich regions (point 6 in Figure 10). An elevated niobium content was also found in the middle zone of the scale (point 2 and 4 in Figure 10). The chemical composition of the alloy after 25 oxidation cycles at 950 °C (point 7 in Figure 10) did not differ from the chemical composition in the initial state (Figure 6).

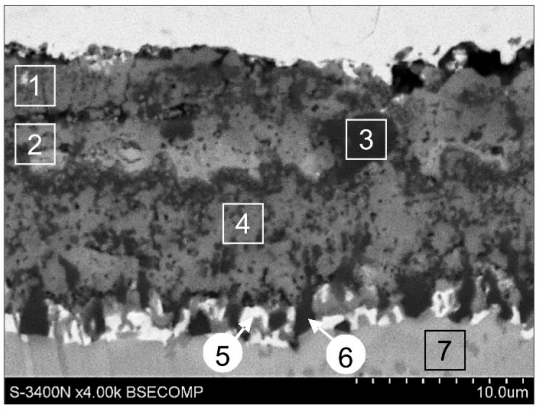


| Area Point | Elements content, at.% | | | |
|---|---|---|---|---|
| | Ti | Al | Nb | O* |
| 1 | 23.4 | 7.8 | 2.9 | 65.9 |
| 2 | 22.1 | 5.8 | 5.5 | 66.6 |
| 3 | 2.1 | 36.2 | 0.9 | 60.8 |
| 4 | 25.2 | 2.5 | 5.2 | 67.1 |
| 5 | 14.5 | 12.5 | 7.2 | 65.8 |
| 6 | 4.0 | 31.5 | 2.7 | 61.8 |
| 7 | 48.7 | 42.0 | 9.3 | - |

* - determined based on stoichiometry

**Figure 10.** The microstructure (SEM) and EDS results (point 1–7) of the oxide scale formed on Ti–45Al–8Nb–0.5(B, C) alloy during 25 cycles of isothermal oxidation at 950 °C.

X-ray diffraction phase composition analysis revealed the presence of $TiO_2$ as the dominant phase within the oxide scale (Figure 11). Also, the presence of $Al_2O_3$ and $AlNbO_4$ was found. Moreover, low intensity peaks of TiN phase were also observed. The peaks from TiAl and $Ti_3Al$ originate from the substrate alloy. Correlation of the XRD results (Figure 11) with chemical composition microanalysis (Figure 10) indicates that $TiO_2$ (rutile) is the predominant phase in the outer layer of the oxide scale, while $Al_2O_3$ was formed mostly at the metal-scale interface. Such a chemical composition of oxide scale, composed maily of $TiO_2$ phase, did not act as a barrier for oxygen even with niobium addition, which seals the anion sublattice of $TiO_2$.

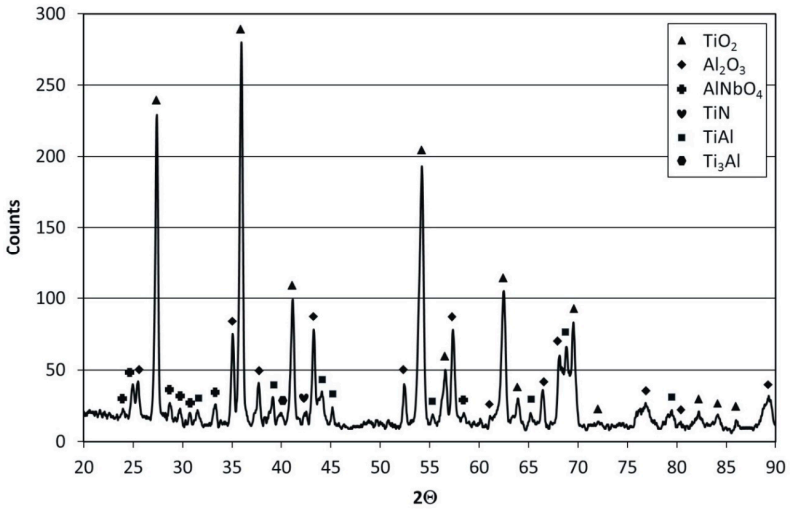


**Figure 11.** X-ray diffractogram of the oxide scale formed on Ti–45Al–8Nb–0.5(B, C) alloy after 25 oxidation cycles at 950 °C.

The application of diffusion aluminizing technology using out-of-pack method allowed for the formation, on a surface of Ti–45Al–8Nb–0.5(B, C) alloy, of a continuous and compact single layer of protective coating of approx. 8 µm of thickness and fine-grained microstructure. The obtained diffuse aluminide coating was characterized by good metallurgical qualities without concavities, pores, delaminations, or cracks.

A considerable mass gain was observed for the aluminized Ti–45Al–8Nb–0.5(B, C) alloy after the first cycle at 950 °C (Figure 9). After second and subsequent cycles, up to 40th cycle, the mass gain was stabilized and lower than that of bare alloy. The oxidation of the alloy with the protective coating is accompanied by a relatively high, although stable, mass growth, resulting in the formation of an adherent scale of significant thickness and compact structure without the propensity for spallation (during the first 40 cycles). The mass gain rate increased after the 40th cycle.

Oxidation curve analysis of investigated alloys and Ti–47Al–2W–0.5Si alloy [25], both of them with aluminide coating deposited by out-of-pack method, shows that isothermal oxidation kinetics in both cases are similar in the range of 60 cycles of the test. After that, the effect of scale growth in case of presented alloy is much higher. The mass gain after 100 cycles of aluminized Ti–45Al–8Nb–0.5(B, C) alloy, which is equivalent to 2300 h of oxidation, was 3.45 mg/cm$^2$ (Figure 9). After 100 cycles, the unit weight gain for Ti–47Al–2W–0.5Si alloy with the coating deposited at the same conditions was approx. 1.7 mg/cm$^2$ [25]. The aluminized Ti–45Al–8Nb–0.5(B, C) alloy did not undergo the breakdown effect after 100 cycles, while it was already observed for the bare alloy after 22 cycles. In both cases, the application of protective coating significantly affected the improvement in their resistance to cyclic oxidation within the entire investigated range.

Macroscopic investigations of the coated alloy revealed the presence of oxide islands marked by olive color (Figure 12). With each subsequent cycle, both the surface fraction of these regions, as well as their size, increased. These observations are in harmony with mass gain measurements (Figure 9).

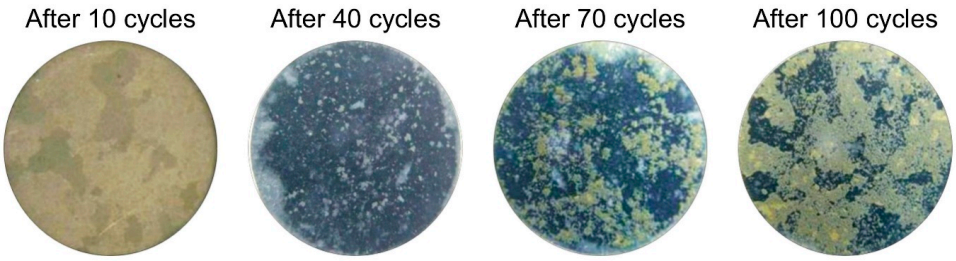


**Figure 12.** The outer surface of the aluminized Ti–45Al–8Nb–0.5(B, C) alloy after cyclic isothermal oxidation at 950 °C.

The depth of the continuous oxide scale on the surface of aluminized Ti–45Al–8Nb–0.5(B, C) after 100 cycles of oxidation at 950 °C is around 30 μm (Figure 13), and this is 3 times greater than in case of Ti–47Al–2W–0.5Si alloy aluminized under the same conditions [25]. The scale is multilayered and of complex structure. The outer layer of the scale is composed of large gray oxides rich in Ti (point 1 in Figure 13) that are present on a continuous and compact Al-rich oxide layer characterized by a dark gray contrast (point 2 in Figure 13). The thickest layer in the middle of the scale consists of Ti-rich bright gray oxides that also contain Al and Nb (point 3 in Figure 13). Between it and a thin Nb-rich layer (point 5 in Figure 13) at the scale-metal interface there are large, dark regions rich in Al of irregular shape (point 4 in Figure 13).

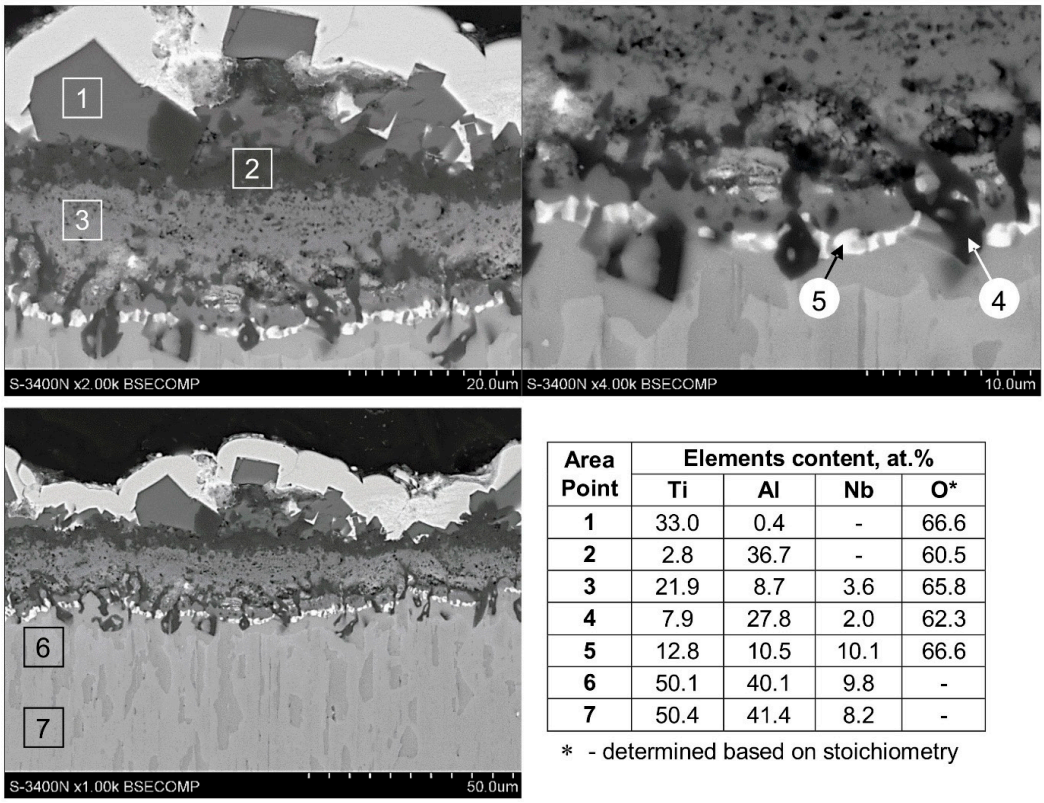


| Area Point | Elements content, at.% | | | |
|---|---|---|---|---|
| | Ti | Al | Nb | O* |
| 1 | 33.0 | 0.4 | - | 66.6 |
| 2 | 2.8 | 36.7 | - | 60.5 |
| 3 | 21.9 | 8.7 | 3.6 | 65.8 |
| 4 | 7.9 | 27.8 | 2.0 | 62.3 |
| 5 | 12.8 | 10.5 | 10.1 | 66.6 |
| 6 | 50.1 | 40.1 | 9.8 | - |
| 7 | 50.4 | 41.4 | 8.2 | - |

* - determined based on stoichiometry

**Figure 13.** The microstructure (SEM) and EDS results of the oxide scale formed on aluminized Ti–45Al–8Nb–0.5(B, C) alloy during 100 cycles of isothermal oxidation at 950 °C.

The ratio of Al content to the sum of Ti and Nb contents in the substrate is close to 1:1. It indicates that the predominant phase in the microstructure of the alloy is TiAl in form of a secondary solid solution containing Nb. The content of Al in the surface layer (points 6 and 7 in Figure 13) is significantly lower than in the initial state, which results in an intensive Al depletion during the cyclic oxidation test.

The changes in oxidation kinetics observed after 40 cycles, which are related to the formation of an undesired $TiO_2$ oxide, do not cause a significant increase in the coating's degradation process, which is the effect of a good adherence of the $Al_2O_3$ scale.

The results of X-ray diffraction phase identification of the oxide scale formed on the aluminized Ti–45Al–8Nb–0.5(B, C) alloy revealed its complex multiphase structure (Figure 14). The XRD pattern contains very strong peaks from $TiO_2$, which is predominant in the oxide scale; strong peaks from $Al_2O_3$; relatively strong (considering the thickness of the scale) peaks from intermetallic phases γ-TiAl and $\alpha_2$-$Ti_3Al$, which constitute the substrate alloy; and weak and single peaks from a complex $Al_2TiO_5$ oxide and TiN nitride. No peaks from phases that form the initial microstructure of the aluminide coating—such as $Al_2Ti$ and $Al_3Ti$—were found (Figure 8). This proves that scale during cyclic oxidation forms at the expense of total and continuous depletion of the protective coating based on Al-rich phases without any signs of pitting corrosion. The obtained results indicate a complete depletion of the protective coating due to the formation of oxides such as $Al_2O_3$ and $Al_2TiO_5$. The presence of notable amounts of $Al_2O_3$ after 100 cycles of oxidation proves its dominant role in providing high oxidation resistance to the aluminized Ti–45Al–8Nb–0.5(B, C) alloy.

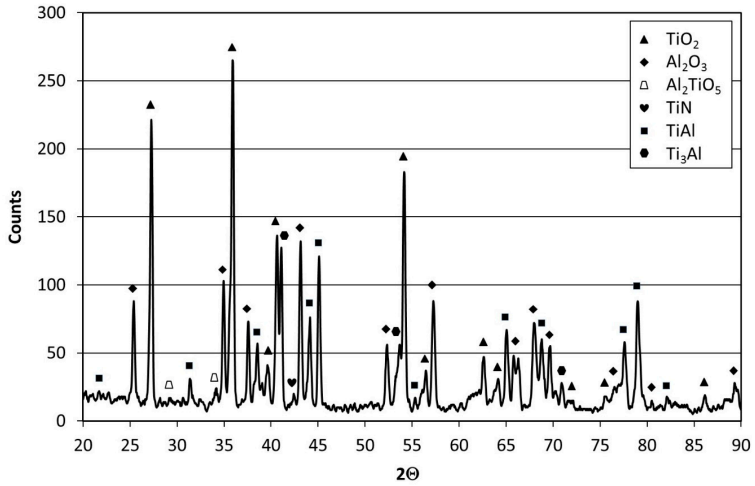


**Figure 14.** X-ray diffractogram of the oxide scale formed on aluminized Ti–45Al–8Nb–0.5(B, C) alloy after 100 oxidation cycles at 950 °C.

## 4. Conclusions

- The compact and tight aluminum coating produced by the "out of pack" method on the surface of the Ti–45Al–8Nb–0.5(B, C) alloy affects the significant improvement of resistance to cyclic oxidation at 950 °C.
- The composition of coating consisting mainly of $Al_2Ti$ and $Al_3Ti$ phases guarantees production of compact, based on the $Al_2O_3$ scale in the oxidation process, which has no tendency to fall.
- The increase in oxidation kinetics (after 50 cycles) is associated with the formation of undesired $TiO_2$ oxide. This occurrence does not cause a significant increase in the coating's degradation process, which is a result of tightness and good adherence of previously formed $Al_2O_3$ scale.
- The favorable behavior of the Ti–45Al–8Nb–0.5(B, C) alloy with a protective coating under cyclic oxidation conditions is the result of a higher content of $Al_2O_3$ in the microstructure of the scale and the presence of Al and Nb-rich phases at the interface with the substrate, which are probably the barrier for the oxidation process.

**Acknowledgments:** Work was partially supported by National Centre for Research and Development, Poland (project no NR15-0019-10).

**Author Contributions:** W.S. conceived the experiments; G.M., A.S. and R.S. performed the experiments; W.S. and G.M. analyzed the data; A.S. contributed reagents/materials; W.S. and A.S. wrote the paper.

**Conflicts of Interest:** The authors declare no conflict of interest.

## References

1. Loria, E.A. Gamma titanium aluminides as prospective structural materials. *Intermetallics* **2000**, *8*, 1339–1345. [CrossRef]
2. Wu, X. Review of alloy and process development of TiAl alloys. *Intermetallics* **2006**, *14*, 1114–1122. [CrossRef]
3. Clemens, H.; Smarsly, W. Light-weight intermetallic titanium aluminides—Status of research and development. *Adv. Mater. Res.* **2011**, *278*, 551–556. [CrossRef]
4. Appel, F.; Paul, J.D.H.; Oehring, M. *Gamma Titanium Aluminide Alloys: Science and Technology*; Wiley-VCH Verlag GmbH & Co. KGaA: Weinheim, Germany, 2011; ISBN 978-3-527-31525-3.
5. Clemens, H.; Mayer, S. Design, processing, microstructure, properties, and applications of advanced intermetallic TiAl alloys. *Adv. Eng. Mater.* **2013**, *15*, 191–215. [CrossRef]
6. Bartolotta, P.; Barrett, J.; Kelly, T.; Smashey, R. The use of cast Ti–48Al–2Cr–2Nb in jet engines. *J. Met.* **1997**, *5*, 48–76. [CrossRef]
7. Tetsui, T. Application of TiAl in a turbocharger for passenger vehicles. *Adv. Eng. Mater.* **2001**, *3*, 307–310. [CrossRef]
8. Wu, X.; Huang, A.; Hu, D.; Loretto, M.H. Oxidation-induced embrittlement of TiAl alloys. *Intermetallics* **2009**, *17*, 540–552. [CrossRef]
9. Brady, M.P. The oxidation and protection of gamma titanium aluminides. *J. Met.* **1996**, *11*, 46–50. [CrossRef]
10. Grabke, H.J. Oxidation of aluminides. *Mater. Sci. Forum.* **1997**, *149*, 251–254. [CrossRef]
11. Haanappel, V.A.C.; Clemens, H.; Stroosnijder, M.F. The high temperature oxidation behaviour of high and low alloyed TiAl-based intermetallics. *Intermetallics* **2002**, *10*, 293–305. [CrossRef]
12. Lee, D.-B. Effect of Cr, Nb, Mn, V, W and Si on high temperature oxidation of TiAl alloys. *Metals Mater. Int.* **2005**, *11*, 141–147. [CrossRef]
13. Lin, J.P.; Zhao, L.L.; Li, G.Y.; Zhang, L.Q.; Song, X.P.; Ye, F.; Chen, G.L. Effect of Nb on oxidation behavior of high Nb containing TiAl alloys. *Intermetallics* **2011**, *19*, 131–136. [CrossRef]
14. Yin, W.M.; Lupinc, V.; Battezzati, L. Microstructure study of a γ-TiAl based alloy containing W and Si. *Mater. Sci. Eng. A* **1997**, *239*, 713–721. [CrossRef]
15. Singheiser, L.; Niewolak, L.; Flesch, U.; Shemet, V.; Quadakkers, W.J. Fundamental considerations for the development of oxidation-resistant alloys and coatings based on γ-TiAl. *Metall. Mater. Trans. A* **2003**, *34*, 2247–2251. [CrossRef]
16. Braun, R.; Fröhlich, M.; Leyens, C. Oxidation behaviour of TiAl-based intermetallic coatings on γ-TiAl alloys. *Int. J. Mater. Res.* **2010**, *101*, 637–647. [CrossRef]
17. Tang, Z.; Wang, F.; Wu, W. Effect of MCrAlY overlay coatings on oxidation resistance of TiAl intermetallics. *Surf. Coat. Technol.* **1998**, *99*, 248–252. [CrossRef]
18. Mabuchi, H.; Asai, T.; Nakayama, Y. Aluminide coatings on TiAl compound. *Scr. Metall.* **1989**, *23*, 685–689. [CrossRef]
19. Góral, M.; Swadźba, L.; Moskal, G.; Hetmańczyk, M.; Tetsui, T. Si-modified aluminide coatings deposited on $Ti_{46}Al_7Nb$ alloy by slurry method. *Intermetallics* **2009**, *17*, 965–967. [CrossRef]
20. Tang, Z.; Wang, F.; Wu, W. Effect of $Al_2O_3$ and enamel coatings on 900 °C oxidation and hot corrosion behaviors of gamma-TiAl. *Mater. Sci. Eng. A* **2000**, *276*, 70–75. [CrossRef]
21. Zhu, Y.-C.; Zhang, Y.; Li, X.Y.; Fujita, K.; Iwamoto, N. The influence of magnetron-sputtered $SiO_2$ coatings on the cyclic oxidation behavior of γ-TiAl alloys. *Mater. Trans. JIM* **2000**, *9*, 1118–1120. [CrossRef]
22. Yoshimura, M.; Urushihara, W.; Yashima, M.; Kakihana, M. $CaTiO_3$ coating on TiAl by hydrothermal-electrochemical technique. *Intermetallics* **1995**, *3*, 125–128. [CrossRef]
23. Żurek, Z.; Stawiarski, A.; Jaroń, A.; Gil, A. Formation and oxidation behaviour of diffusion-barrier-coating system on γ-TiAl. *ECS Trans.* **2011**, *33*, 17–22.

24. Góral, M.; Moskal, G.; Swadźba, L. Gas phase aluminizing of TiAl intermetallics. *Intermetallics* **2009**, *17*, 669–671. [CrossRef]
25. Szkliniarz, A.; Moskal, G.; Szkliniarz, W.; Swadźba, R. Improvement of oxidation resistance of Ti–47Al–2W–0.5Si alloy modified by aluminizing method. *Surf. Coat. Technol.* **2015**, *277*, 270–277. [CrossRef]
26. Goral, M.; Swadźba, L.; Moskal, G.; Jarczyk, G.; Aguilar, J. Diffusion aluminide coatings for TiAl intermetallic turbine blades. *Intermetallics* **2011**, *19*, 744–747. [CrossRef]
27. Szkliniarz, W.; Szkliniarz, A. The chemical composition and microstructure of Ti–47Al–2W–0.5Si alloy melted in ceramic crucibles. *Solid State Phenom.* **2012**, *191*, 211–220. [CrossRef]
28. Szkliniarz, W.; Szkliniarz, A. Quantitative characterization of microstructure of Ti–47Al–2W–0.5Si alloy after melting in vacuum induction furnace. *Solid State Phenom.* **2013**, *197*, 113–118. [CrossRef]




© 2018 by the authors. Licensee MDPI, Basel, Switzerland. This article is an open access article distributed under the terms and conditions of the Creative Commons Attribution (CC BY) license (http://creativecommons.org/licenses/by/4.0/).